Journal of Molecular Catalysis A: Chemical 304 (2009) 191–198

Contents lists available at ScienceDirect

Journal of Molecular Catalysis A: Chemical

journal homepage: www.elsevier.com/locate/molcata

Ni(II) and Ru(II) Schiff base complexes as catalysts for the reduction of benzene

V. Arun[a,1], N. Sridevi[b], P.P. Robinson[a,1], S. Manju[a,1], K.K.M. Yusuff[a,*]

[a] Department of Applied Chemistry, Cochin University of Science and Technology, Cochin 682022, Kerala, India
[b] Department of Chemistry, School of Science and Humanities, VIT University, Vellore 632014, Tamilnadu, India

ARTICLE INFO

Article history:
Received 8 January 2009
Received in revised form 5 February 2009
Accepted 7 February 2009
Available online 20 February 2009

Keywords:
Schiff base complex
Ruthenium(II)
Nickel(II)
Catalysis
Benzene hydrogenation

ABSTRACT

Two new complexes, $[M^{II}(L)(Cl)(H_2O)_2]\cdot H_2O$ (where M = Ni or Ru and L = heterocyclic Schiff base, 3-hydroxyquinoxaline-2-carboxalidene-4-aminoantipyrine), have been synthesized and characterized by elemental analysis, FT-IR, UV–vis diffuse reflectance spectroscopy, FAB-MASS, TG–DTA, AAS, cyclic voltammetry, conductance and magnetic susceptibility measurements. The complexes have a distorted octahedral structure and were found to be effective catalysts for the hydrogenation of benzene. The influence of several reaction parameters such as reaction time, temperature, hydrogen pressure, concentration of the catalyst and concentration of benzene was tested. A turnover frequency of 5372 h^{-1} has been found in the case of ruthenium complex for the reduction of benzene at 80 °C with 3.64×10^{-6} mol catalyst, 0.34 mol benzene and at a hydrogen pressure of 50 bar. In the case of the nickel complex, a turnover frequency of 1718 h^{-1} has been found for the same reaction with 3.95×10^{-6} mol catalyst under similar experimental conditions. The nickel complex shows more selectivity for the formation of cyclohexene while the ruthenium complex is more selective for the formation of cyclohexane.

1. Introduction

Hydrogenation of aromatic compounds to aliphatic cyclic products is an important reaction with potential applications in chemical industry [1–8]. Health risks related to aromatic compounds, such as benzene and some polyaromatic compounds have encouraged legislators to tighten the restrictions on aromatic content in fuels and solvents. Reduction of benzene is of immense application in the industry, as the product, cyclohexene, is used as a raw material for the production of adipic acid and caprolactam, both of which are intermediates used in the production of Nylon 6 and Nylon 66 [9]. Various metal-based catalysts including those of ruthenium and nickel have been extensively used for the partial and complete reduction of benzene [10–20].

The catalytic reduction of benzene nucleus generally requires more severe conditions than that of simple olefins [21]. Even though a lot of success has been achieved with regard to transition metal complex catalyzed hydrogenation of olefins [22–25], there are only few reports on studies involving hydrogenations of arenes using homogeneous metal complex catalysts [26–32]. A few homogeneous ruthenium-based catalysts have been prepared and used as catalysts for hydrogenation of aromatics [33–39]. It is therefore considered as challenge to prepare new and effective homogeneous catalysts for hydrogenation of aromatic compounds. We have synthesized two new complexes, having the general molecular formula, $[M^{II}(L)(Cl)(H_2O)_2]\cdot H_2O$, where M = Ni or Ru and L = 3-hydroxyquinoxaline-2-carboxalidene-4-aminoantipyrine, which exhibited excellent catalytic activity towards the hydrogenation of benzene. The results of these studies are presented in this paper.

2. Experimental

2.1. Materials

$RuCl_3\cdot 3H_2O$ and $NiCl_2\cdot 6H_2O$ purchased from Sigma–Aldrich Chemicals Private Limited (Bangalore, India), were used as-supplied. All other chemicals used were analytical reagent grade. Organic solvents used were purified and dried by standard methods. Hydrogen gas with >99.8% purity supplied by Sterling Gases Ltd. (Cochin, India), was used as such.

2.2. Synthesis of the ligand

The details regarding the synthesis and characterisation of the Schiff base ligand, 3-hydroxyquinoxaline-2-carboxalidene-4-aminoantipyrine (L), is given as the supplementary information.

* Corresponding author. Tel.: +91 484 2575804.
E-mail addresses: yusuff@cusat.ac.in, yusuff15@yahoo.com (K.K.M. Yusuff).
[1] Tel.: +91 484 2575804.

1381-1169/$ – see front matter © 2009 Elsevier B.V. All rights reserved.
doi:10.1016/j.molcata.2009.02.011

2.3. Synthesis of the $[Ru^{II}(L)(Cl)(H_2O)_2]\cdot H_2O$

The ligand, L (1 mmol, 0.36 g) was dissolved in an aqueous solution (250 mL) of NaOH (1 mmol, 0.04 g). A solution of $RuCl_3\cdot 3H_2O$ (1 mmol, 0.26 g) in water (25 mL) was added drop-wise to this solution of the ligand. The yellowish green complex separated was filtered and washed with 1:9 methanol–water (to remove any salts) and with diethylether. It was then dried in vacuum over anhydrous calcium chloride in a desiccator.

Yield: 80%. Anal. Calcd. for $C_{20}H_{22}ClN_5O_5Ru$ (548.94): C, 43.76; H, 4.04; N, 12.76; Cl, 6.46; Ru, 18.41. Found: C, 43.70; H, 3.98; N, 12.71; Cl, 6.41; Ru, 17.99. Λ_M (DMF, $ohm^{-1}\,cm^2\,mol^{-1}$): 4.20.

2.4. Synthesis of the $[Ni^{II}(L)(Cl)(H_2O)_2]\cdot H_2O$

A procedure similar to that of the synthesis of ruthenium complex was adopted for preparation of the nickel complex using $NiCl_2\cdot 6H_2O$ (1 mmol, 0.24 g). The complex separated has an orange red colour.

Yield: 86%. Anal. Calcd. for $C_{20}H_{22}ClN_5O_5Ni$ (506.56): C, 47.42; H, 4.38; N, 13.83; Cl, 7.00; Ni, 11.59. Found: C, 47.30; H, 4.25; N, 13.76; Cl, 6.89; Ni, 11.45. Λ_M (DMF, $ohm^{-1}\,cm^2\,mol^{-1}$): 4.36.

2.5. Methods

Microanalyses of the compounds were done with an Elementar Vario EL III CHNS elemental analyzer. Room-temperature FT-IR spectra were recorded as KBr pellets with a JASCO FTIR 4100 Spectrophotometer in the 4000–400 cm^{-1} range and far-IR spectrum of the complex was recorded using polyethylene pellets in the 500–100 cm^{-1} region on a Nicolet Mega 550 FTIR Instrument. Electronic spectrum of the ligand was recorded on a Thermoelectron Nicolet Evolution 300 UV-Vis spectrophotometer. Diffuse reflectance spectra of the complexes were recorded at room temperature in a Jasco V 570 UV-Vis spectrophotometer in the wavelength range 200–1800 nm with a scanning rate 200 nm/min. Absorbance spectra were obtained from the reflectance spectra by means of Kubelka–Munk transformations. FAB mass spectra were recorded at room temperature on a JEOL SX 102/DA-6000 mass spectrometer in *m*-nitrobenzyl alcohol matrix. X-band EPR spectra of the ruthenium complex were taken in solid state and in DMF at LNT using Varian E-112 X/Q band spectrophotometer. The molar conductivity of the complex was measured using a Systronic conductivity bridge type 305 in DMSO. Chlorine was estimated gravimetrically using the standard procedure [40] after fusing the complex in sodium carbonate/sodium peroxide mixture. Estimation of nickel and ruthenium was carried out on a Thermo Electron Corporation, M series Atomic Absorption Spectrophotometer. Magnetic susceptibility measurements were done at room temperature on a Magway MSB Mk 1 Magnetic Susceptibility Balance. TG–DTA analysis was carried out under air and nitrogen with a heating rate of 20 °C/min using a Perkin Elmer Pyres Diamond TG/DTA analyser. Cyclic voltammetric studies of the ruthenium complex in acetonitrile were carried out with a BAS EPSILON Electrochemical Analyser using glassy-carbon working electrode with a scan rate of 100 mV/s. A Pt wire and Ag/AgCl were used as counter and reference electrodes, respectively.

All catalytic runs were carried out in a 100 mL bench top mini-reactor made of stainless steel 316 (Autoclave Engineers, Division of Snap-tite, Inc. PA). Hydrogenation was performed by charging the reactor with known quantities of the catalyst and benzene. Air was flushed out of the reactor with low-pressure of hydrogen, after which the inlet valve was closed and heating commenced with stirring at 600 rpm. When the designated temperature was reached, hydrogen was fed to the reactor to a predetermined pressure, which was maintained throughout the reaction with the help of a mass flow meter. The reaction was carried out for 2 h over the pressure range 10–50 bar, temperature range 60–140 °C, varying the catalyst from 1.0 to 3.0 mg and benzene concentration from 9.36 to 15.60 mol l^{-1}. During the run, samples (about 0.5 mL each) were withdrawn periodically and analyzed using a Chemito 8510 Gas Chromatograph with FID detector. The column used was Chromosorb W and nitrogen was used as the carrier gas. Products of the reaction were identified by using Varian 1200 L Single Quadrupole GC–MS with helium as the carrier gas and VF-5MS as column.

3. Results and discussion

During the complexation step an equivalent amount of aqueous NaOH was added to the ligand to convert the iminol –OH to enolate form, which renders the coordination of enolate oxygen and easy separation of the complexes. The ruthenium complex separates as a yellowish green and the nickel complex as orange red solid. Both the complexes are stable in air and are soluble in methanol, dichloromethane, acetonitrile, benzene, toluene, DMF and DMSO. However, our attempts to prepare single crystals suitable for X-ray crystal structure determination were not successful.

3.1. Elemental analysis and FAB mass spectrum

The elemental analyses show that the molecular formula of the nickel complex is $[Ni(L)(Cl)(H_2O)_2]\cdot H_2O$ and that of the ruthenium complex is $[Ru(L)(Cl)(H_2O)_2]\cdot H_2O$. FAB mass spectrum of the nickel complex shows the molecular ion peak at $m/z = 506$, which is in agreement with the elemental analysis data. The peaks observed at *m*/*z*, 488, 470, 452 and 417 correspond to $[NiLCl(H_2O)_2]^+$, $[NiLCl(H_2O)]^+$, $[NiLCl]^+$ and $[NiL]^+$ respectively. For the ruthenium complex, molecular ion peak observed at $m/z = 549$ agrees with the formula obtained from the elemental analysis. The peaks at *m*/*z*, 531, 513, 495 and 460 can be attributed due to $[RuLCl(H_2O)_2]^+$, $[RuLCl(H_2O)]^+$, $[RuLCl]^+$ and $[RuL]^+$ respectively. In both cases the peak at *m*/*z*, 360 is due to the free ligand moiety.

Magnetic moment of the Ni(II) complex is 2.76 BM, which suggests a high-spin octahedral structure for the complex [41]. Although we used $RuCl_3\cdot 3H_2O$ for the synthesis, the complex is formed in the 2+ oxidation state, which is evident from the molecular formula, $[Ru(L)(Cl)(H_2O)_2]\cdot H_2O$ and the diamagnetic and EPR silent nature of the complex.

3.2. Cyclic voltammetry of the ruthenium complex

The cyclic voltammograms of the ligand and $[Ru^{II}(L)(Cl)(H_2O)_2]\cdot H_2O$ at 300 K were taken to have more insight into the oxidation state of the ruthenium and are shown in Fig. 1. Concentration of the ligand as well as that of the complex was 5×10^{-5} mol l^{-1} and the supporting electrolyte used was tetra n-butylammonium hexafluorophosphate (0.1 mol l^{-1}). The solution was purged with a continuous flow of N_2 gas before scanning.

Cyclic voltammogram of the ligand displayed a quasi-reversible redox process with a peak-to-peak separation 203 mV. The reduction occurs at a cathodic peak potential of −0.873 V (E_{pc}) and oxidation occurs upon scan reversal at an anodic potential of −0.670 V (E_{pa}). Therefore the ligand is susceptible to easy oxidation and reduction, which might be the reason for the formation of the ruthenium(II) complex. The less negative value of reduction potential for this ligand compared to other pyrazine derivatives, such as 2,3-bis(2′-pyridyl)-pyrazine ($E_{1/2} = -1.80$ V), 2,3-bis(2′-pyridyl)-quinoxaline ($E_{1/2} = -1.43$ V), 2,3-di(2′-pyridyl)(benzo(g)quinoxaline) ($E_{1/2} = -1.29$ V) and 6,7-dichloro-2,3-bis(2′-pyridyl)-quinoxaline (−1.18 V) [42–44], may be due to the presence of the oxygen atoms directly bonded to the pyrazine ring of the ligand.

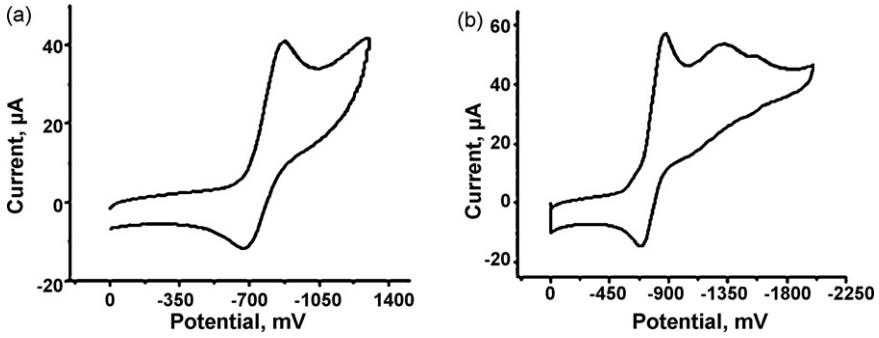

Fig. 1. Cyclic voltammograms of: (a) the ligand and (b) the $[Ru^{II}(L)(Cl)(H_2O)_2]\cdot H_2O$ in acetonitrile at 300 K.

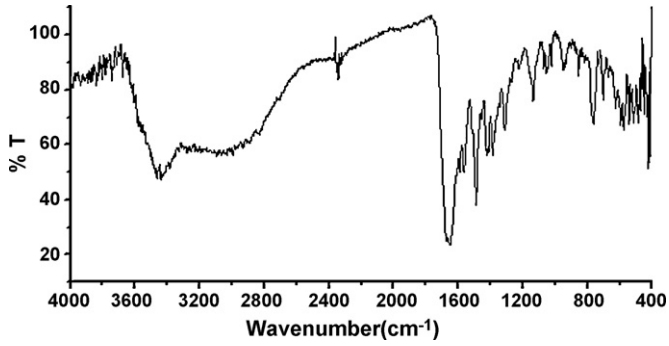

Fig. 2. FT-IR spectrum of $[Ru^{II}(L)(Cl)(H_2O)_2]\cdot H_2O$.

Cyclic voltammogram of the ruthenium complex shows two quasi-reversible redox processes occurring at negative potential and with a peak-to-peak separation (ΔE_p value) of 182 and 209 mV respectively [22]. The first redox process occurs with the cathodic peak potential at −0.870 V (E_{pc}) and anodic peak potential at −0.688 V (E_{pa}) and peaks for the second redox process occur at a higher negative value (E_{pc} = −1.314 V and E_{pa} = −1.105 V) suggesting the ligand-centred nature for the process. Due to this ligand-centred nature, the peak potentials for Ru(II)/Ru(III) couple get shifted to more negative potential.

3.3. Infrared spectra

IR spectra of the complexes are given in Figs. 2 and 3. The free ligand exhibit amide-iminol tautomerism and in the solid-state amide form predominates which is evidenced by a strong ν(C=O) band at 1670 cm^{-1} [45]. The ligand is coordinated to the metal through the enolate oxygen in the iminol form. This coordination is evidenced by the changes in the phenolic ν(C–O) stretching observed at 1306 cm^{-1} in the free Schiff base. On complexation this band is shifted to 1312 cm^{-1} in the spectrum of ruthenium complex and to 1310 cm^{-1} in the spectrum of nickel complex [46]. The band at 1656 cm^{-1} due to the C=O group of the antipyrine part of the ligand is shifted to 1650 cm^{-1} in complexes indicating the involvement of this group in coordination [47]. The ligand contains different types of ν(C=N) bonds and they are not well resolved in the spectrum. The azomethine –CH=N band is superimposed with that of the C=O group of the amide tautomer and appears as a weak band at 1637 cm^{-1} in the case of free ligand. The participation of azomethine nitrogen atom in chelation is evidenced by an increase of the stretching frequency to 1670 cm^{-1}. This increase in azomethine stretching frequency on coordination might be due to the extensive delocalization of the π-electrons in fully conjugated Schiff base ligand. The weak bands corresponding to the C=N of the quinoxaline rings are seen in the range 1616–1565 cm^{-1}. The coordination of phenolic oxygen is supported by the appearance of a band at 448 cm^{-1} due to Ru–O stretching in the ruthenium complex [48]. The new band observed at 444 cm^{-1} may be due to the ν(Ni–O) of the nickel complex [49]. In addition, the ν(M–N) stretch in the ruthenium and nickel complexes appears as a strong band at 426 and 246 cm^{-1} respectively [48,50]. The band observed at 325 cm^{-1} in the far-IR spectrum of the complex might be due to the ν(Ru–Cl) [51]. For the ruthenium complex, δ(O–H) of the coordinated water molecules are observed at 1162 and 1185 cm^{-1} and the ν(O–H) is observed as a broad band at 3442 cm^{-1} [52]. In the case of nickel complex, the δ(O–H) appears at 1163 and 1173 cm^{-1} and the ν(O–H) at 3421 cm^{-1} as a broad band [53].

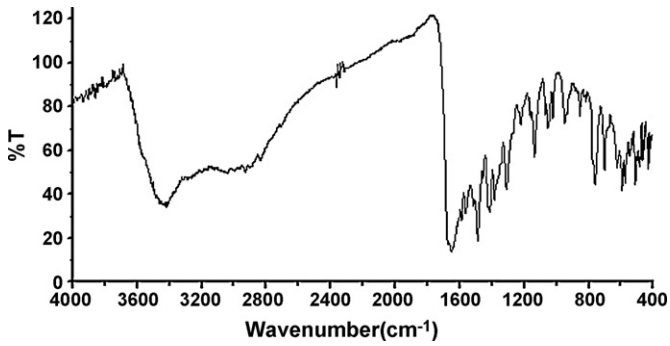

Fig. 3. FT-IR spectrum of $[Ni^{II}(L)(Cl)(H_2O)_2]\cdot H_2O$.

3.4. Electronic spectra

The electronic spectra of the complexes were recorded in the solution state and in the solid state. In solution spectrum, the ligand-centered bands gets dominated and hence d–d bands could not be observed. The solution spectra of the ligand and its nickel and ruthenium complexes (10^{-4} mol l^{-1}) in acetonitrile are shown in Fig. 4. But in the solid-state diffuse reflectance spectra, the d–d bands were seen due to the high concentration of the complexes.

The diffused reflectance spectra of the ruthenium and nickel complexes are shown in Figs. 5 and 6. The ground state of ruthenium(II) in an octahedral environment is $^1A_{1g}$, arising from the t_{2g}^6 configuration. The excited states corresponding to the $t_{2g}^5e_g^1$ configuration are $^3T_{1g}$, $^3T_{2g}$, $^1T_{1g}$ and $^1T_{2g}$. Hence, four bands corresponding to the transitions $^1A_{1g} \rightarrow {}^3T_{1g}$, $^1A_{1g} \rightarrow {}^3T_{2g}$, $^1A_{1g} \rightarrow {}^1T_{1g}$ and $^1A_{1g} \rightarrow {}^1T_{2g}$ are possible in the order of increasing energy. The transition $^1A_{1g} \rightarrow {}^1T_{2g}$ is not observed in the present complex, as it might have been masked by the charge transfer band at 486 nm (20 570 cm^{-1}). The shoulder bands observed at 645 nm (15 500 cm^{-1}), 840 nm (11,900 cm^{-1}) and 1422 nm (7030 cm^{-1}) might be due to $^1A_{1g} \rightarrow {}^1T_{1g}$ and spin forbidden $^1A_{1g} \rightarrow {}^3T_{2g}$ and $^1A_{1g} \rightarrow {}^3T_{1g}$ transitions respectively.

For octahedral/pseudo-octahedral nickel(II) complexes, the crystal field theory allows for three spin allowed d–d transitions,

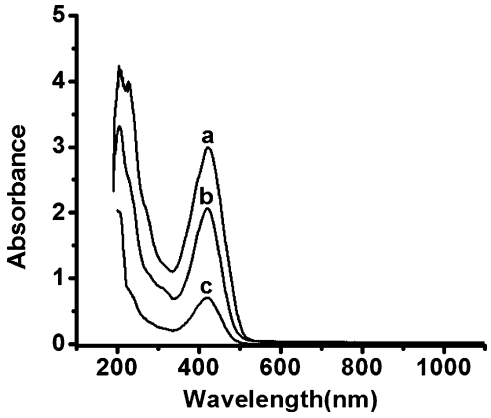

Fig. 4. UV–vis spectra of: (a) the $[Ni^{II}(L)(Cl)(H_2O)_2]\cdot H_2O$, (b) $[Ru^{II}(L)(Cl)(H_2O)_2]\cdot H_2O$, and (c) ligand in acetonitrile.

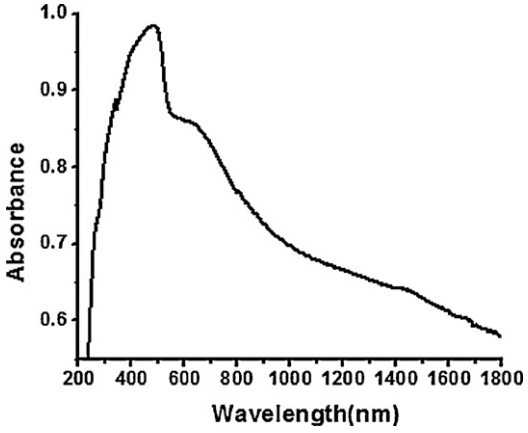

Fig. 5. Diffuse reflectance spectrum of $[Ru^{II}(L)(Cl)(H_2O)_2]\cdot H_2O$.

namely $^3A_{2g}(F) \rightarrow {}^3T_{2g}(F)$, $^3A_{2g}(F) \rightarrow {}^3T_{1g}(F)$ and $^3A_{2g}(F) \rightarrow {}^3T_{1g}(P)$ [54]. The first two bands appear over the near-IR range 6940–9520 cm^{-1} corresponding to transitions $^3A_{2g}(F) \rightarrow {}^3T_{2g}(F)$ and $^3A_{2g}(F) \rightarrow {}^3T_{1g}(F)$ respectively. In the visible region of the spectrum only one band corresponding to $^3A_{2g}(F) \rightarrow {}^3T_{1g}(P)$ transition appears at 20 830 cm^{-1}. Besides this, two spin forbidden transitions ($^3A_{2g}(F) \rightarrow {}^1E_g(D)$ and $^3A_{2g}(F) \rightarrow {}^1T_{2g}(D)$) are often observed in the case of octahedral nickel(II) complexes and the position of these bands can be either close to the lowest energy spin allowed transition to the $^3T_{2g}$ state or close to $^3T_{1g}$ [55]. Here the band observed at 5980 cm^{-1} may be due to the spin-forbidden $^3A_{2g}(F) \rightarrow {}^1E_g(D)$ transition.

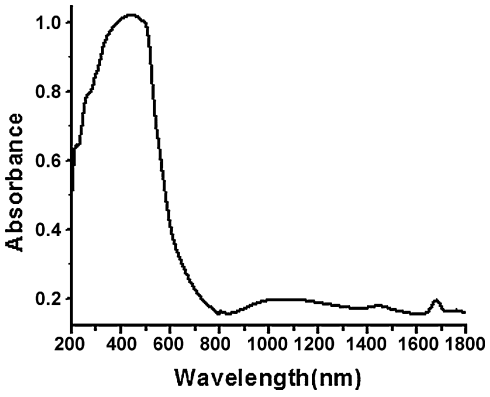

Fig. 6. Diffuse reflectance spectrum of $[Ni^{II}(L)(Cl)(H_2O)_2]\cdot H_2O$.

3.5. Thermal analysis

Thermal stability of the complexes was investigated using TG–DTA at a heating rate of 20 °C/min in nitrogen/air over a temperature range of 40–1000 °C. TG–DTA curves of $[Ru^{II}(L)(Cl)(H_2O)_2]\cdot H_2O$ are shown in Fig. 7. In the nitrogen atmosphere the mass loss up to 85 °C (calc. 3.28%; found 3.10%) is due to the loss of lattice water. A mass loss in the temperature range 85–240 °C (calc. 6.02%; found 5.92%) corresponds to the loss of two coordinated water molecules. The mass loss due to the removal of coordinated chlorine occurs in the temperature range 240–280 °C (calc. 6.25%; found 6.10%), followed by the decomposition of ligand, which takes place in two steps. The decomposition was not seen to be completed even after 1000 °C. DTA study reveals that all the decomposition stages are exothermic in nature. TG curve recorded in air is almost similar in nature; however the decomposition takes place at lower temperatures. The final residue was found to be RuO (calc. 21.32%; found 20.72%).

The TG–DTA thermograms of $[Ni^{II}(L)(Cl)(H_2O)_2]\cdot H_2O$ are shown in Fig. 8. In nitrogen, a loss of weight in the temperature range 40–130 °C (calc. 3.56%; found 3.20%) is due to the loss of lattice water. The two coordinated water molecules are seen to lose in the temperature range 130–250 °C (calc. 7.11%; found 6.92%) followed by the removal of coordinated chlorine in the range 250–305 °C (calc. 7.00%; found 6.86%). Then the decomposition of the ligand takes place and was not seen to be completed even after 1000 °C. Thermal decomposition of the complex in air takes place at a lower temperature and the residue was found to be NiO.

Based on the above analytical data and physicochemical properties, an octahedral structure is proposed for these nickel(II) and ruthenium(II) complexes (Fig. 9). The octahedral coordination is satisfied by two water molecules, one chlorine atom and hydroxyl oxygen, azomethine nitrogen and oxygen of the pyrazoline ring of the ligand.

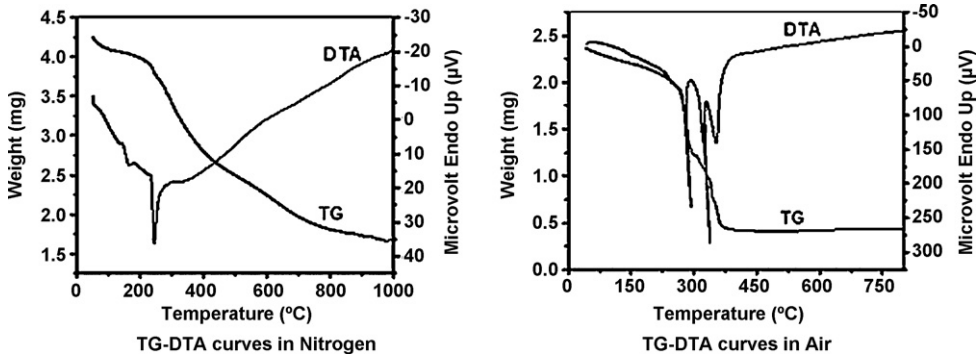

Fig. 7. TG–DTA curves of $[Ru^{II}(L)(Cl)(H_2O)_2]\cdot H_2O$.

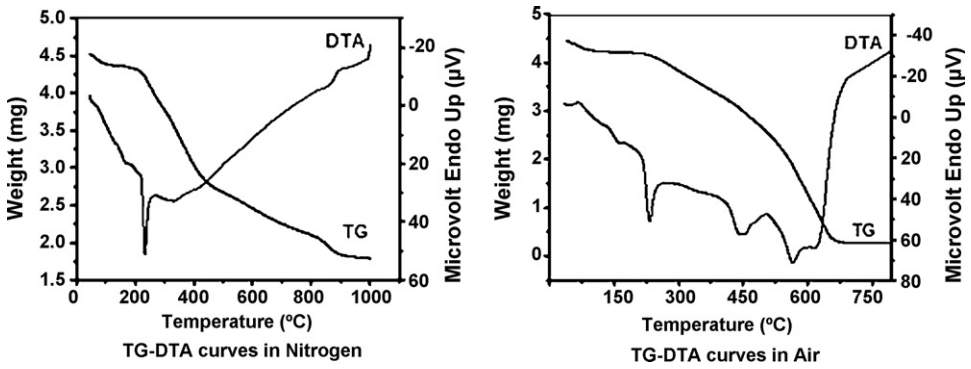

Fig. 8. TG–DTA curves of $[Ni^{II}(L)(Cl)(H_2O)_2]\cdot H_2O$.

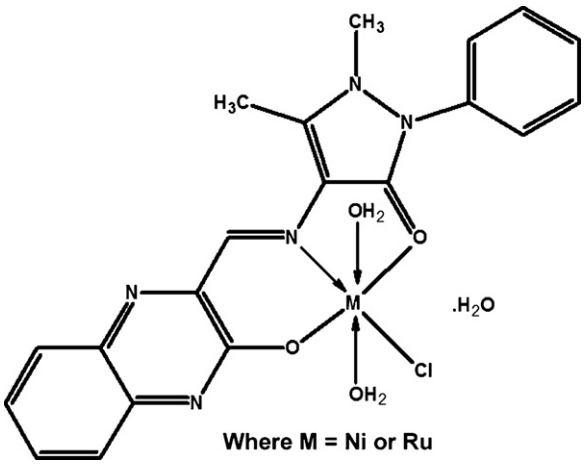

Fig. 9. Proposed structures for the complexes.

3.6. Catalytic activity towards the hydrogenation of benzene

The partial and complete reduction of benzene results in the formation of cyclohexene and cyclohexane respectively (Scheme 1). The activity of some common metals towards the hydrogenation of benzene and alkyl benzene decreases in the order Rh > Ru > Pt > Ni > Pd > Co [56]. We carried out benzene hydrogenation using $[Ru^{II}(L)(Cl)(H_2O)_2]\cdot H_2O$ and $[Ni^{II}(L)(Cl)(H_2O)_2]\cdot H_2O$ complexes as catalysts. A detailed catalytic study towards the reduction of benzene using these complexes was carried out under solvent free condition by carrying out runs at different catalyst and substrate concentrations, dihydrogen pressure, reaction time and temperature of reaction mixtures and the data thus obtained are summarized in Tables 1 and 2.

3.6.1. Effect of catalyst concentration

The influence of catalyst concentration on the reduction of benzene was carried out over the range 1–3 mg, while the benzene concentration (0.39 mol), dihydrogen pressure (50 bar) and the temperature (80 °C) were kept constant (Tables 1 and 2). In both cases an increment of the catalyst concentration raises the conversion of benzene (Fig. 10). The selectivity remains almost the same over this concentration range and the nickel catalyst is more selective towards cyclohexene and the ruthenium catalyst shows higher selectivity for cyclohexane.

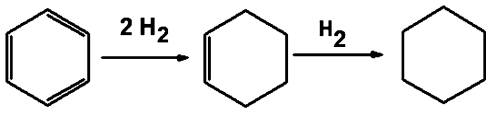

Scheme 1. Formation of cyclohexene and cyclohexane.

3.6.2. Effect of dihydrogen pressure

To analyse the dependence of dihydrogen pressure on the reduction of benzene, a series of experiments were carried out by varying the pressure over the range of 10–50 bar at 80 °C keeping both the initial substrate concentration (0.39 mol) and the catalyst loading (2 mg) constant. A beneficial effect of hydrogen pressure is shown in the hydrogenation of benzene, since the conversion increases from 10 up to 50 bar (Fig. 11). The nickel complex showed a higher selectivity for cyclohexene, whereas the ruthenium complex is more selective for cyclohexane (Tables 1 and 2).

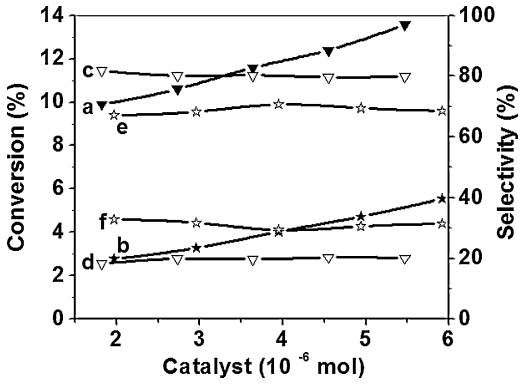

Fig. 10. Effect of catalyst: where a = conversion by $[Ru^{II}(L)(Cl)(H_2O)_2]\cdot H_2O$; b = conversion by $[Ni^{II}(L)(Cl)(H_2O)_2]\cdot H_2O$; c = cyclohexane selectivity for $[Ru^{II}(L)(Cl)(H_2O)_2]\cdot H_2O$; d = cyclohexene selectivity for $[Ru^{II}(L)(Cl)(H_2O)_2]\cdot H_2O$; e = cyclohexene selectivity for $[Ni^{II}(L)(Cl)(H_2O)_2]\cdot H_2O$; f = cyclohexane selectivity for $[Ni^{II}(L)(Cl)(H_2O)_2]\cdot H_2O$.

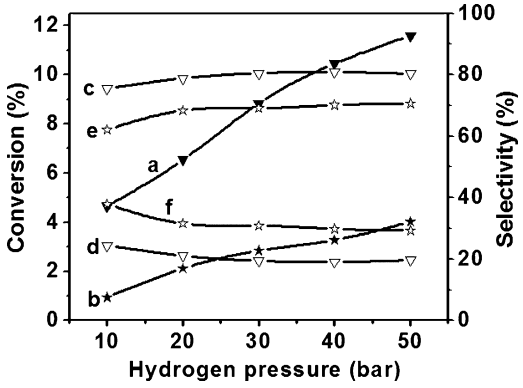

Fig. 11. Effect of pressure, where a–f are the same as those in Fig. 10.

Table 1
Summary of the $[Ru^{II}(L)(Cl)(H_2O)_2]\cdot H_2O$ catalyzed hydrogenation of benzene.

[Catalyst] (10^{-6} mol)	[Benzene] (mol)	H_2 pressure (bar)	Temperature (°C)	Conversion (%)	Selectivity (%)	
					Cyclohexane	Cyclohexene
3.64	0.34	10	80	4.7	75	25
3.64	0.34	20	80	6.5	79	21
3.64	0.34	30	80	8.8	81	19
3.64	0.34	40	80	10.4	81	19
3.64	0.34	50	80	11.6	80	20
3.64	0.39	50	80	10.8	82	18
3.64	0.45	50	80	10.3	84	16
3.64	0.51	50	80	9.9	86	14
3.64	0.56	50	80	9.1	86	14
1.82	0.34	50	80	9.9	82	18
2.73	0.34	50	80	10.6	80	20
4.55	0.34	50	80	12.4	80	20
5.47	0.34	50	80	13.6	80	20
3.64	0.34	50	60	5.1	78	22
3.64	0.34	50	100	12.8	82	18
3.64	0.34	50	120	14.5	82	18
3.64	0.34	50	140	20.7	82	18

General reaction conditions: 0.34 mol benzene, 80 °C temperature, 50 bar dihydrogen pressure, 3.64×10^{-6} mol catalyst, 600 rpm stirring speed, and 2 h reaction time. Turnover frequency (TOF) is the mol of benzene transformed per mol of the catalyst per hour. For the general conditions the TOF of the ruthenium complex is 5372 h^{-1}.

Table 2
Summary of the $[Ni^{II}(L)(Cl)(H_2O)_2]\cdot H_2O$ catalyzed hydrogenation of benzene.

[Catalyst] (10^{-6} mol)	[Benzene] (mol)	H_2 pressure (bar)	Temperature (°C)	Conversion (%)	Selectivity (%)	
					Cyclohexane	Cyclohexene
3.95	0.34	10	80	1.0	38	62
3.95	0.34	20	80	2.1	32	68
3.95	0.34	30	80	2.9	31	69
3.95	0.34	40	80	3.3	30	70
3.95	0.34	50	80	4.0	29	71
3.95	0.39	50	80	3.4	28	72
3.95	0.45	50	80	2.7	26	74
3.95	0.51	50	80	2.4	24	76
3.95	0.56	50	80	2.0	23	77
1.97	0.34	50	80	2.8	33	67
2.96	0.34	50	80	3.3	32	68
4.94	0.34	50	80	4.7	31	69
5.92	0.34	50	80	5.5	31	69
3.95	0.34	50	60	1.4	29	71
3.95	0.34	50	100	4.6	29	71
3.95	0.34	50	120	4.1	36	64
3.95	0.34	50	140	3.6	43	57

General reaction conditions: 0.34 mol benzene, 80 °C temperature, 50 bar dihydrogen pressure, 3.95×10^{-6} mol catalyst, 600 rpm stirring speed, and 2 h reaction time. Turnover frequency (TOF) is the mol of benzene transformed per mol of the catalyst per hour. For the general conditions the TOF of the nickel complex is 1718 h^{-1}.

3.6.3. Effect of benzene concentration

The effect of benzene concentration (Fig. 12) was studied in the range 0.34–0.56 mol at a constant catalyst concentration of 2 mg at 80 °C and at 50 bar pressure (Tables 1 and 2). In the case of ruthenium catalyst, percentage conversion decreases, whereas percentage selectivity for cyclohexane and cyclohexene remains the same with increase in the concentration of benzene. The nickel complex is more selective for cyclohexene and this selectivity increases with increase in the benzene concentration. However the percentage reduction of benzene shows a decrease as the concentration of benzene increases.

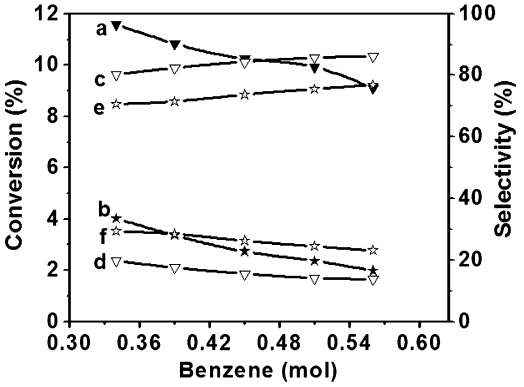

Fig. 12. Effect of benzene, where a–f are the same as those in Fig. 10.

3.6.4. Effect of reaction time

In order to study the effect of time, reaction was carried out for 4 h with 2 mg of catalyst, 0.39 mol benzene, and 50 bar dihydrogen pressure at 80 °C with a stirring speed of 600 rpm. The products were analysed at 30 min interval and the results are shown in Fig. 13. Conversion of benzene linearly increased with increase in time. In both catalysts at the beginning the selectivity of cyclohexene is larger and then decreases as the time elapses. This means that the benzene is first hydrogenated to cyclohexene and then to cyclohexane.

3.6.5. Effect of temperature

The reduction of benzene was also studied at various temperatures in the range 60–140 °C with 2 mg samples of the nickel and ruthenium complexes, keeping all other parameters constant. It was observed that for the same temperature, the percentage reduction

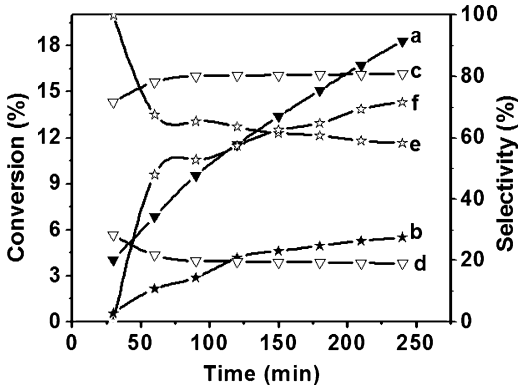

Fig. 13. Effect of time, where a–f are the same as those in Fig. 10.

of benzene is greater for the ruthenium catalyst than that for the nickel complex (Fig. 14). In the case of ruthenium complex, cyclohexane selectivity increases up to 100 °C and then remains almost constant. A reverse trend is observed in the cyclohexene selectivity for the ruthenium complex (Table 1). Table 2 shows that the nickel complex shows a maximum conversion at 100 °C and then decreases. However, the selectivity of cyclohexene in the case of nickel complex remains almost the same up to 100 °C and then decreases with further increase in temperature. Thus for the same temperature the nickel complex is more selective for cyclohexene formation and the ruthenium complex gives higher selectivity to cyclohexane formation.

Generally benzene can be hydrogenated directly to cyclohexane or through an intermediate cyclohexene. Here we got both cyclohexene and cyclohexane as the products. This suggests that the benzene is first converted to cyclohexene and then to cyclohexane. In the case of the ruthenium complex, formation of cyclohexene and the further reduction of it to cyclohexane take place at a faster rate. This results in the formation of cyclohexane as the major product. In the case of nickel catalyst the partial hydrogenated product, cyclohexene, is the major product and at low temperature the partial hydrogenation predominates.

For the general condition (0.34 mol benzene, 80 °C temperature, 50 bar hydrogen pressure, 2 mg of the catalyst, and 600 rpm stirring speed) the TOF of the ruthenium and nickel complex is 5372 and 1718 h^{-1} respectively. This value is much higher than that reported for some of the mononuclear ruthenium-based catalysts for the homogeneous hydrogenation of arenes [30,57].

We carried out the same reaction under identical conditions without the catalyst, with the organic ligand, with $NiCl_2{\cdot}6H_2O$ and with $RuCl_3{\cdot}3H_2O$. In all these three cases no hydrogenation product was detected at the end of the reaction. These results proved that the hydrogenation was catalyzed by the added complex catalysts. Finke and co-workers [1,58,59] reported that the hydrogenation of benzene under vigorous conditions (50–100 °C) using metal complexes proceeds through the formation of M(0) nanoclusters, which are not seen by naked eye. We have carried out the hydrogenation of benzene using the Ni(II) and Ru(II) complexes in the temperature range 60–140 °C. At 80 °C the nickel complex gives a conversion with a turnover frequency of 1718 h^{-1}. This hydrogenation activity cannot be due to Ni(0), as it is not possible to reduce Ni(II) complex to Ni(0) at 80 °C. Further in the case of ruthenium complex, at the end of the reaction there were no black particles of ruthenium metal in the reaction mixture and the addition of mercury, as a selective poison for colloidal/nanoparticle catalysts, to the reaction system does not significantly affect the percentage conversion of benzene. From these evidences we conclude that the benzene hydrogenation in our system proceeds through a homogeneous mechanism and not through the formation of M(0) nanoparticles.

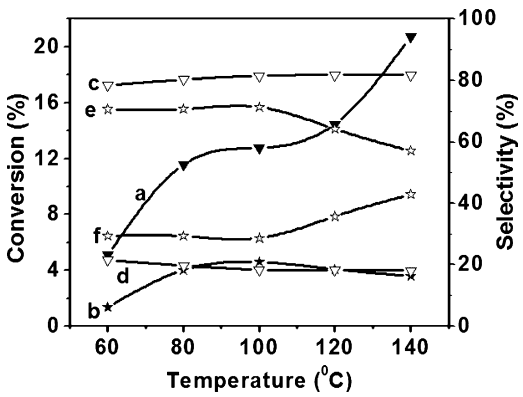

Fig. 14. Effect of temperature, where a–f are the same as those in Fig. 10.

4. Conclusion

An octahedral structure has been assigned for these complexes with general molecular formula $[M^{II}(L)(Cl)(H_2O)_2]{\cdot}H_2O$, where M is Ni or Ru and L = 3-hydroxyquinoxaline-2-carboxalidene-4-aminoantipyrine. These complexes were shown to be efficient catalysts for the reduction of benzene. Compared to the nickel complex catalyst, the ruthenium complex gives a higher conversion with a turnover frequency of 5372 h^{-1} under identical experimental conditions. The ruthenium catalyst is more selective towards cyclohexane, while the nickel catalyst is more selective for cyclohexene. At 80 °C the nickel complex gives a conversion with a turnover frequency of 1718 h^{-1}.

Acknowledgements

The authors thank Department of Science and Technology, India, for using the Sophisticated Analytical Instrumentation Facility (SAIF) at CDRI, Lucknow (for FAB-MAS spectral data and EPR measurement), at Indian Institute of Technology, Bombay (for far-IR spectrum) and at Sophisticated Test & Instrumentation Centre, Cochin University of Science and Technology, Cochin (for GC–MS and elemental analyses). We also thank Dr. A. Ajayaghosh, NIIST, Trivandrum, Kerala for the ^1H NMR and ^{13}C NMR spectra. S.M. thanks Kerala State Council for Science, Technology and Environment, Kerala, India, for research fellowship.

Appendix A. Supplementary data

Supplementary data associated with this article can be found, in the online version, at doi:10.1016/j.molcata.2009.02.011.

References

[1] J.A. Widegren, R.G. Finke, J. Mol. Catal. A: Chem. 191 (2003) 187–207.
[2] G.C. Bond, Appl. Catal. 41 (1988) 313–335.
[3] L.P. Lindfors, T. Salmi, Ind. Eng. Chem. Res. 32 (1993) 34–42.
[4] C. Morin, D. Simon, P. Sautet, Surf. Sci. 600 (2006) 1339–1350.
[5] P.A. Rautanen, J.R. Aittamaa, A. Outi, I. Krause, Ind. Eng. Chem. Res. 39 (2000) 4032–4039.
[6] M.C. Rakowski, F.J. Hirsekorn, L.S. Stuhl, E.L. Muetterties, Inorg. Chem. 15 (1976) 2379–2382.
[7] A. Stanislaus, B.H. Cooper, Catal. Rev. Sci. Eng. 36 (1) (1994) 75–123.
[8] S. Toppinen, T.K. Rantakyla, T. Salmi, J. Aittamaa, Ind. Eng. Chem. Res. 35 (1996) 1824–1833.
[9] K. Weissermel, H.-J. Arpe, Industrial Organic Chemistry, VCH, New York, 1993; G.W. Parshall, S.D. Ittel, The applications and chemistry of catalysis by soluble transition metal complexes, in: Homogeneous Catalysis, 2nd ed., Wiley, New York, 1992.
[10] J. Wang, Y. Wang, S. Xie, M. Qiao, H. Li, K. Fan, Appl. Catal. A: Gen. 272 (2004) 29–36.
[11] J. Struijk, R. Moene, T. Van der Kamp, J.J.F. Scholten, Appl. Catal. A 89 (1992) 77.

[12] J. Struijk, M. D'Angremond, W.J.M. Lucas-De Regt, J.J.F. Scholten, Appl. Catal. A 83 (1992) 263.
[13] S.-C. Hu, Y.-W. Chen, J. Chem. Technol. Biotechnol. 76 (2001) 954–958.
[14] P. Kluson, L. Cerveny, J. Mol. Catal. A: Chem. 108 (1996) 107–112.
[15] P.J. Baricelli, L. Izaguirre, J. Lopez, E. Lujano, F. Lopez-Linares, J. Mol. Catal. A: Chem. 208 (2004) 67–72.
[16] B. Chen, U. Dingerdissen, J.G.E. Krauter, H.G.J. Lansink Rotgerink, K. Mobus, D.J. Ostgard, P. Panster, T.H. Riermeier, S. Seebald, T. Tacke, H. Trauthwein, Appl. Catal. A: Gen. 280 (2005) 17–46.
[17] D.U. Parmar, S.D. Bhatt, H.C. Bajaj, R.V. Jasra, J. Mol. Catal. A: Chem. 202 (2003) 9–15.
[18] P.G. Savva, K. Goundani, J. Vakros, K. Bourikas, Ch. Fountzoula, D. Vattis, A. Lycourghiotis, Ch. Kordulis, Appl. Catal. B: Environ. 79 (2008) 199–207.
[19] M.S. Lylykangas, P.A. Rautanen, A.O.I. Krause, Ind. Eng. Chem. Res. 41 (2002) 5632–5639.
[20] S. Lu, W.W. Lonergan, J.P. Bosco, S. Wang, Y. Zhu, Y. Xie, J.G. Chen, J. Catal. 259 (2008) 260–268.
[21] J. March, Advanced Organic Chemistry: Reactions, Mechanisms, and Structure, 4th ed., Wiley-Interscience, New York, 1992, p. 780.
[22] A. Andriollo, A. Bolivar, F.A. Ldpez, D.E. Pdez, Inorg. Chim. Acta 238 (1995) 187–192.
[23] P.J. Baricelli, G. Rodriguez, M. Rodriguez, E. Lujano, F. Lopez-Linares, Appl. Catal. A: Gen. 239 (2003) 25–34.
[24] C. Daguenet, R. Scopelliti, P.J. Dyson, Organometallics 23 (2004) 4849–4857.
[25] D.G. Holah, A.N. Hughes, B.C. Hui, C.T. Kan, J. Catal. 48 (1977) 340–344.
[26] I.M. Angulo, E. Bouwman, J. Mol. Catal. A: Chem. 175 (2001) 65–72.
[27] I.M. Angulo, S.M. Lok, V.F. Quiroga Norambuena, M. Lutz, A.L. Spek, E. Bouwman, J. Mol. Catal. A: Chem. 187 (2002) 55–67.
[28] C. Daguenet, P.J. Dyson, Catal. Commun. 4 (2003) 153–157.
[29] C.R. Landis, J. Halpern, Organometallics 2 (1983) 840–842.
[30] A.F. Borowski, S. Sabo-Etienne, B. Chaudret, J. Mol. Catal. A: Chem. 174 (2001) 69–79.
[31] J.A. Widegren, M.A. Bennett, R.G. Fink, J. Am. Chem. Soc. 125 (34) (2003) 10301–10310.
[32] E.L. Muetterties, J.R. Bleeke, Acc. Chem. Res. 12 (9) (1979) 324–331.
[33] C.P. Lau, S.M. Ng, G. Jia, Z. Lin, Coord. Chem. Rev. 251 (2007) 2223–2237.
[34] R. Drozdzak, B. Allaert, N. Ledoux, I. Dragutan, V. Dragutan, F. Verpoort, Coord. Chem. Rev. 249 (2005) 3055–3074.
[35] K. Abdur-Rashid, S.E. Clapham, A. Hadzovic, J.N. Harvey, A.J. Lough, R.H. Morris, J. Am. Chem. Soc. 124 (2002) 15104–15118.
[36] R. Noyori, S. Hashiguchi, Acc. Chem. Res. 30 (1997) 97–102.
[37] K. Nomura, H. Ogura, Y. Imanishi, J. Mol. Catal. A: Chem. 178 (2002) 105–114.
[38] K. Nomura, H. Ogura, Y. Imanishi, J. Mol. Catal. A: Chem. 166 (2001) 345–349.
[39] C.A. Sandoval, T. Ohkuma, K. Muniz, R. Noyori, J. Am. Chem. Soc. 125 (2003) 13490–13503.
[40] A.I. Vogel, A Text Book of Quantitative Inorganic Analysis, 3rd ed., Longman, London, 1978.
[41] F.A. Cotton, G. Wilkinson, Advanced Inorganic Chemistry, Wiley-Interscience, New York, 1962.
[42] S.M. Molnar, K.R. Neville, G.E. Jensen, K.J. Brewer, Inorg. Chim. Acta 206 (1993) 69–76.
[43] S. Roffia, M. Marcaccio, C. Paradisi, F. Paolucci, V. Balzani, G. Denti, S. Serroni, S. Campagna, Inorg. Chem. 32 (14) (1993) 3003–3009.
[44] D.L. Carlson, W.R. Murphy Jr., Inorg. Chim. Acta 181 (1991) 61–64.
[45] V. Arun, P.P. Robinson, S. Manju, P. Leeju, G. Varsha, V. Digna, K.K.M. Yusuff, Dyes and Pigments (2009), doi:10.1016/j.dyepig.2009.01.010.
[46] K. Veno, A.E. Maetell, J. Phys. Chem. 60 (1956) 1230.
[47] R.M. Issa, A.M. Khedr, H.F. Rizk, Spectrochim. Acta: Part A 62 (2005) 621–629.
[48] K. Nakamoto, Infrared and Raman Spectra of Inorganic and Coordination Compounds, 4th ed., John Wiely and Sons, Inc, New York, 1986.
[49] B.S. Garg, D.N. Kumar, Spectrochim. Acta: Part A 59 (2003) 229–234.
[50] K. Kurdziel, T. Glowiak, Polyhedron 19 (2000) 2183–2188.
[51] M.M. Taqui Khan, N.H. Khan, R.I. Kureshy, A.B. Boricha, Z.A. Shaikh, Inorg. Chim. Acta 170 (1990) 213–223.
[52] S.M.E. Khalil, M.M. Mashaly, A.A.A. Emara, Synth. React. Inorg. Met. Org. Chem. 25 (8) (1995) 1373–1389.
[53] S.S. Kandil, Trans. Met. Chem. 23 (1998) 461–465.
[54] A.B.P. Lever, Inorganic Electronic Spectroscopy, 2nd ed., Elsevier, New York, 1984.
[55] E. Gonzalez, A. Rodrigue-Witchel, C. Reber, Coord. Chem. Rev. 251 (2007) 351–363.
[56] R.L. Augustine, Heterogeneous Catalysis for the Synthetic Chemist, Marcel Dekker, New York, 1996 (Chapter 17).
[57] L. Zhang, Y. Zhang, X.-G. Zhou, R.-X. Li, X.-J. Li, K.C. Tin, N.-B. Wong, J. Mol. Catal. A: Chem. 256 (2006) 171–177.
[58] C.M. Hagen, J.A. Widegren, P.M. Maitlis, R.G. Finke, J. Am. Chem. Soc. 127 (2005) 4423–4432.
[59] Y. Lin, R.G. Finke, Inorg. Chem. 33 (1994) 4891–4910.